SAGE

ICRP
Annals of the ICRP

The reference phantoms: voxel vs polygon

C.H. Kim[a], Y.S. Yeom[a], T.T. Nguyen[a], Z.J. Wang[a], H.S. Kim[a], M.C. Han[a], J.K. Lee[a], M. Zankl[b], N. Petoussi-Henss[b], W.E. Bolch[c], C. Lee[d], B.S. Chung[e]

[a]*Department of Nuclear Engineering, Hanyang University, 133-791, 222 Wangsimni-ro, Seongdong-gu, Seoul, Republic of Korea; e-mail: chkim@hanyang.ac.kr*
[b]*Helmholtz Zentrum München Deutsches Forschungszentrum für Gesundheit und Umwelt (GmbH), Germany*
[c]*University of Florida, USA*
[d]*National Cancer Institute, USA*
[e]*Ajou University School of Medicine, Republic of Korea*

Abstract–The International Commission on Radiological Protection (ICRP) reference male and female adult phantoms, described in *Publication 110*, are voxel phantoms based on whole-body computed tomography scans of a male and a female patient, respectively. The voxel in-plane resolution and the slice thickness, of the order of a few millimetres, are insufficient for proper segmentation of smaller tissues such as the lens of the eye, the skin, and the walls of some organs. The calculated doses for these tissues therefore present some limitations, particularly for weakly penetrating radiation. Similarly, the *Publication 110* phantoms cannot represent 8–40-μm-thick target regions in respiratory or alimentary tract organs. Separate stylised models have been used to represent these tissues for calculation of the ICRP reference dose coefficients (DCs). ICRP Committee 2 recently initiated a research project, the ultimate goal of which is to convert the *Publication 110* phantoms to a high-quality polygon-mesh (PM) format, including all source and target regions, even those of the 8–40-μm-thick alimentary and respiratory tract organs. It is expected that the converted phantoms would lead to the same or very similar DCs as the *Publication 110* reference phantoms for penetrating radiation and, at the same time, provide more accurate DCs for weakly penetrating radiation and small tissues. Additionally, the reference phantoms in the PM format would be easily deformable and, as such, could serve as a starting point to create phantoms of various postures for use, for example, in accidental dose calculations. This paper will discuss the current progress of the phantom conversion project and its significance for ICRP DC calculations.

This paper does not necessarily reflect the views of the International Commission on Radiological Protection.

Keywords: Reference phantom; Voxel; Polygon mesh; Effective dose

1. INTRODUCTION

The International Commission on Radiological Protection (ICRP) adult male and female reference phantoms, which were adopted by ICRP in its 2007 Recommendations (ICRP, 2007), are now used for organ and effective dose calculations by ICRP (2010) and researchers. These phantoms (ICRP, 2009) were developed using whole-body computed tomography data of a male and a female patient, and are consistent with the data given in *Publication 89* (ICRP, 2002) on the reference anatomical and physiological parameters for male and female. Compared with stylised phantoms, these phantoms are anatomically more realistic; they have, however, some limitations in representing organs and tissues that are complex or very thin. This is mainly due to the fact that these phantoms are defined by cuboid-shaped voxels, the resolution of which is not adequate for all purposes. The voxel sizes of the male and female phantoms are $2.137\,\text{mm} \times 2.137\,\text{mm} \times 8\,\text{mm}$, and $1.775\,\text{mm} \times 1.775\,\text{mm} \times 4.8\,\text{mm}$, respectively (ICRP, 2009). With these large voxels, complex or thin organs or tissues cannot be modelled or defined properly, causing limitations in dose calculation, especially for weakly penetrating radiations.

The skin of the *Publication 110* (ICRP, 2009) reference phantoms, for example, is represented by one layer of voxels and has many holes; this is anatomically incorrect, incurring significant error in dose calculation for charged particles. In addition, the shallow depth (50–100 μm) at which the cells at risk are located cannot be realised by the given voxel dimensions. Hollow organs such as the stomach, urinary bladder, and gall bladder also have many holes. Moreover, the target layers of the respiratory and alimentary tract organs, which are very thin tissues (i.e. 8–40 μm), cannot be modelled in the *Publication 110* reference phantoms, again due to the limitations of the voxel resolution. For all abovementioned regions, separate calculations of specific absorbed fraction (SAF) were performed using stylised phantoms (ICRP, 1994, 2006). Furthermore, the lens of the eye could not be represented properly in the *Publication 110* phantoms. Therefore, for calculating the lens dose coefficients (DCs) for some geometries and energies of external beams of photons and electrons, additional calculations were performed using a stylised phantom (ICRP, 2010). Concerning the skeletal tissues, there are a few further minor problems. For instance, some spongiosa is not covered by cortical bone, part of the cartilage is included in the spongiosa, and the sacrum of the female phantom does not have any cortical bone.

These problems were discussed at the ICRP Committee 2 meeting in 2013, and the decision was made to initiate a research project to convert the *Publication 110* reference phantoms to a high-quality polygon-mesh (PM) format. Prior to that meeting, a preliminary study had confirmed the feasibility of the conversion (Yeom et al., 2013). For the conversion project, a working group was established at Hanyang University in Seoul, Korea in December 2013, and necessary research funding was

secured from the Nuclear Safety and Security Commission through the Korea Foundation of Nuclear Safety in December 2014. The objective of the research project, as noted above, was to produce exact replicas of the current *Publication 110* reference phantoms in high-quality PM format to address the aforementioned problems. This paper will seek to discuss the current progress of the phantom conversion project and its significance in ICRP DC calculations.

2. MATERIALS AND METHODS

2.1. Construction of simple organs

To construct PM models of simple organs, the voxel models of the *Publication 110* reference phantoms were converted directly to the PM format. For this, two conversion procedures were developed: one for very simple organs and the other for more complex organs. For very simple organs, the voxel model is first used to generate a PM model using a three-dimensional surface rendering method. Next, the number of polygons in the PM model is increased to facilitate the smoothing and refinement processes. After completion of the smoothing and refinement processes, the number of facets is reduced to a proper number. The number of facets for an organ model is selected rather arbitrarily, considering the shape of the organ model; that is, for high efficiency in computer simulations, the minimum necessary number of facets to keep the shape of the organ is used. Finally, the shape of the constructed organ model is finely adjusted to the voxel model according to the acceptance criteria used here for organ adjustment.

Two acceptance criteria were developed and applied to the adjustment process. The first criterion was the Dice index (DI), which is simply the volume overlap fraction of two different models (Dice, 1945). For confirmation of successful adjustment, the DI should be greater than 97% of the maximally achievable volume overlap fraction (MAVOF) for a given organ. Note that the MAVOF exists for a given organ due to the fundamental difference in the geometry format (i.e. voxel vs PM). The second criterion was the centroid distance (CD), which is the distance between the centroids of the voxel model and the PM model. For confirmation of successful adjustment, the CD should be less than 0.5 mm.

The conversion process for more complex organs is similar to the process for very simple organs. The only difference is that, during the conversion process, the PM model is converted to the Non-Uniform Rational B-Spline (NURBS) format. The NURBS surface is subsequently converted back to the PM format and subjected to the adjustment process.

2.2. Construction of the skeletal system

The same methods to produce the PM models of simple bones (humeri, ulnae, clavicles, femora, tibiae, mandible, pelvis, scapulae, sacrum, sternum, cranium, and ribs) were used for simple organs. The cranium was complicated, so a more elaborate adjustment process was involved. Each of the 24 ribs was converted and adjusted individually.

Production of a high-quality spine model by the direct conversion methods proved difficult. Therefore, in this case, a pre-existing high-quality PM spine model (Shin et al., 2012) was adopted and adjusted to the voxel spine model, monitoring both the DI and the CD. The same method was used for the hands and the feet.

The *Publication 110* female phantom has toe-standing feet, while the male phantom has normal-standing feet; therefore, the feet of the female phantom were modified to the normal-standing form. The cartilage that had been included incorrectly in spongiosa was extracted and included in the residual tissue. Although this is still not anatomically correct, this approach is believed to be more appropriate, considering that cartilage is not a target tissue, and that the composition and mass density of the cartilage are very close to those of the residual tissue. The costal cartilage and intervertebral discs were modelled following the method used during the construction of the University of Florida/National Cancer Institute (UF/NCI) phantoms (Lee et al., 2010). Cortical bone was added to the sacrum of the female phantom. The male sacrum of the original voxel model did not have the dorsal sacral foramina, and holes were therefore added to the PM model.

2.3. Construction of complex organs

Phantom construction of complex organs such as the eyes, lymphatic nodes, small intestine, muscle, lungs, and blood vessels is very challenging and time consuming, and proper construction methods are still in development. Similarly, the definition of target layers in the alimentary and respiratory tract organs is also challenging. Therefore, target layers were classified here as complex organs.

The detailed model of the eye developed by Behrens et al. (2009), which was adopted for calculations of DC for external beams (ICRP, 2010), has been successfully reproduced and incorporated in the PM phantoms. First, a NURBS-surface-based eye model was produced from the geometrical information of the detailed model of the eye (Behrens et al., 2009) using Rhinoceros software (Robert McNeel & Associates, Seattle, WA, USA). The NURBS model produced was subsequently converted to the PM format. Defects in the eye model were repaired by means of several refinement functions of Rapidform software (INUS Technology Inc., Seoul, Korea). The detailed procedure can be found in Nguyen et al. (2015).

The lymphatic nodes of the *Publication 110* reference phantoms could not be converted directly to the PM format due to their complexity and distribution throughout the body. A dedicated computer programme was developed to model them in the PM phantoms, following the method used for the UF/NCI phantoms (Lee et al., 2009). The developed programme will be used to generate the lymphatic nodes after the construction of muscles is completed.

Construction of the model of the small intestine is also very challenging, again due to the complexity of the structures. A dedicated procedure and computer programme have been developed to generate the model of the small intestine in the PM phantoms. First, a surface frame that entirely encloses the original voxel model of the small intestine is constructed with the α-shape algorithm (Edelsbrunner et al., 1983).

Next, a C^{++} programme developed here is used to automatically generate a small intestine passage line using the Monte Carlo approach. Along with the passage line, a model of the small intestine is generated in the PM format. Finally, the surface is copied for use as the interior surface, which is then reduced to match the reference volumes of the wall and contents, as these are given in *Publication 89* (ICRP, 2002). The aforementioned procedure is repeated 1000 times, randomly producing 1000 different models of the small intestine, and the best model is selected considering both geometric and dosimetric similarity. This method has been applied to produce the model of the small intestine for the male phantom (Yeom et al., 2015). The same method will be used for the female phantom.

2.4. Calculation of DCs

Dose calculations have been performed using the preliminary versions of the phantoms in order to test the proposed approach for the skeletal system and some complex organs. The DCs of the PM phantoms and the *Publication 110* phantoms were calculated using GEometry ANd Tracking 4 (Geant4) Version 10.01 (Agostinelli et al., 2003). The physics library used in Geant4 was the G4EmLivermorePhysics, which includes the Evaluated Photons Data Library (Cullen et al., 1997), the Evaluated Electrons Data Library (Perkins et al., 1991), and the Evaluated Atomic Data Library (Perkins et al., 1997). The secondary production cut value of 0.1 mm was applied for both photons and electrons, with some exceptions where the micron-thick target regions are important in dose calculation. The relative statistical errors were less than 10%.

3. RESULTS AND DISCUSSION

Fig. 1 shows the preliminary PM versions of the *Publication 110* reference phantoms. Table 1 provides the numerical data. Although it is not visible in the figures, several thin target layers of the alimentary tract organs are defined (i.e. oral cavity, oesophagus, stomach, small intestine, and colon). Note that the phantoms described here do not present the final versions, but their external shapes will not change significantly. The lymphatic nodes will be remodelled after construction of the muscles. It can be seen that the male phantom has a model of the small intestine that was constructed here, whereas the female phantom has a stylised model of the small intestine.

Fig. 2 shows the deviation of DCs of the PM phantoms from those of the *Publication 110* reference phantoms for external photons and for red bone marrow (RBM). The RBM DCs were calculated using the mass-weighting approximation, which was used to calculate the *Publication 116* DCs (ICRP, 2010). It can be seen that the deviation is mostly within 5%. Somewhat larger deviation is observed for photon energies below 0.03 MeV, which is due to problems with the original voxel phantoms. In the *Publication 110* reference phantoms, some spongiosa bones are not fully enclosed by the cortical bone, which is anatomically incorrect. The result for endosteum is not given here, but shows a very similar trend.

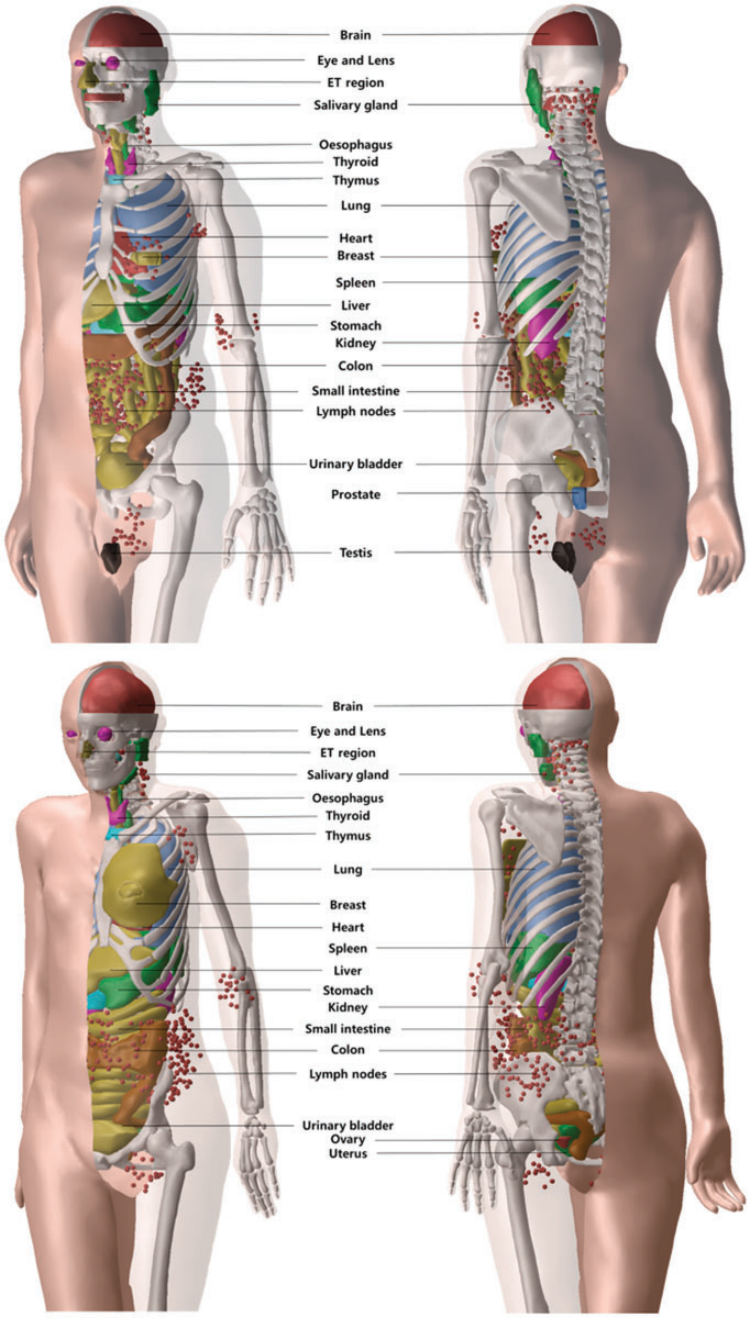

Fig. 1. Polygon-mesh versions (preliminary) of the *Publication 110* (ICRP, 2009) reference phantoms. Top, male phantom; bottom, female phantom. ET, extrathoracic.

Table 1. Numbers of polygon facets and masses of the organs of the polygon-mesh versions (under development) of the *Publication 110* reference phantoms (ICRP, 2009). For comparison, the masses of the organs of the reference male and female are also given, as in *Publication 89* (ICRP, 2002).

	Male				Female			
Organs	Number of facets	Mass (g)	Reference value (g)	Diff. (%)	Number of facets	Mass (g)	Reference value (g)	Diff. (%)
Adrenals	3200	14.00	14	0.00	3000	13.00	13	0.00
Extrathoracic regions	10,100	39.44			19,000	18.61		
Oral mucosa, lips and cheeks	4564	0.02			1720	0.02		
Oral mucosa, roof of mouth	580	0.02			728	0.02		
Oral mucosa, tongue	4192	0.08	73	0.00	5128	0.06	60	0.00
Tongue, upper part (food region)	1232	21.00			2132	21.00		
Tongue, lower part	2096	51.92			2564	38.94		
Trachea	1600	10.00	10	0.00	1600	8.00	8	0.00
Skeleton	604,900	9349.99	10,450	0.00	865,100	6860.00	7760	0.00
Cartilage, costal	18,300	55.54			13,300	41.39		
Cartilage, intervertebral discs	30,000	80.91			26,000	68.41		
Cartilage, rest (in residual soft tissue)		963.56				790.20		
Brain	10,000	1450.00	1450	0.00	10,500	1300.00	1300	0.00
Breasts, adipose tissue	1600	15.00	25	0.00	6800	300.00	500	0.00
Breasts, glandular tissue	1000	10.00			2900	200.00		
Gallbladder wall	1100	10.00	10	0.00	1100	8.00	8	0.00
Gallbladder contents	1100	58.00	58	0.00	1100	48.00	48	0.00
Oesophagus wall	3960	39.90	40	0.00	2984	34.90	35	0.00
Oesophagus wall, target layer	2846	0.10			1492	0.10		

(continued on next page)

Table 1. (continued)

Organs	Male				Female			
	Number of facets	Mass (g)	Reference value (g)	Diff. (%)	Number of facets	Mass (g)	Reference value (g)	Diff. (%)
Oesophagus contents	2846	22.65			1492	21.03		
Stomach wall	12,060	148.70	150	0.00	7602	138.95	140	0.00
Stomach wall, target layer	4030	1.30			2534	1.05		
Stomach contents	4030	250.00	250	0.00	2534	230.00	230	0.00
Small intestine wall	60,000	647.67	650	0.00	32,816	598.01	600	0.00
Small intestine wall, target layer	20,000	2.33			11,036	1.99		
Small intestine contents	20,000	350.00	350	0.00	11,036	280.00	280	0.00
Right colon wall	9534	149.50	150	0.00	4904	144.54	145	0.00
Right colon wall, target layer	6748	0.50			2036	0.46		
Right colon contents	6748	150.00	150	0.00	2036	160.00	160	0.00
Left colon wall	8702	149.60	150	0.00	5368	144.69	145	0.00
Left colon wall, target layer	6000	0.40			2314	0.31		
Left colon contents	6000	75.00	75	0.00	2314	80.01	80	0.01
Rectosigmoid wall	6902	69.67	70	0.00	3422	69.67	70	0.00
Rectosigmoid wall, target layer	5060	0.33			1394	0.33		
Rectosigmoid contents	5060	75.00	75	0.00	1394	79.99	80	−0.01
Heart wall	4000	330.00	330	0.00	6500	250.00	250	0.00
Heart contents (blood)	5000	510.00	510	0.00	5000	370.00	370	0.00
Kidneys	3000	310.00	310	0.00	3300	275.00	275	0.00
Liver	5000	1800.00	1800	0.00	5000	1400.00	1400	0.00
Lungs	13,000	1200.00	1200	0.00	14,000	950.00	950	0.00

(continued on next page)

Table 1. (continued)

Organs	Male				Female			
	Number of facets	Mass (g)	Reference value (g)	Diff. (%)	Number of facets	Mass (g)	Reference value (g)	Diff. (%)
Lymphatic nodes	65,400	178.37			65,400	142.69		
Testes (m)/ovaries (f)	3000	35.00	35	0.00	2000	11.00	11	0.00
Pancreas	2000	140.00	140	0.00	2000	120.00	120	0.00
Pituitary gland	600	0.60	0.6	0.00	620	0.60	0.6	0.00
Prostate (m)/uterus (f)	1000	17.00	17	0.00	2000	80.00	80	0.00
Salivary glands	2500	85.00	85	0.00	8600	70.00	70	0.00
Skin	62,000	3300.00	3300	0.00	65,000	2300.00	2300	0.00
Spinal cord	3000	36.62			1500	18.63		
Spleen	1500	150.00	150	0.00	1500	130.00	130	0.00
Teeth	4452	50.00	50	0.00	1780	40.00	40	0.00
Thymus	1000	25.00	25	0.00	1700	20.00	20	0.00
Thyroid	1600	20.00	20	0.00	1600	17.00	17	0.00
Tonsils	500	3.00	3	0.00	1600	3.00	3	0.00
Urinary bladder wall	1000	50.00	50	0.00	2400	40.00	40	0.00
Urinary bladder contents	1000	200.00			2400	200.00		
Air in the body	1800	0.12			1500	0.05		
Lens of the eye	7424	0.456	0.4	14.00	7424	0.456	0.4	14.00
Eyeballs	22,788	14.756	14.6	1.07	22,788	14.756	14.6	1.07
Residual soft tissue	68,000	51,245.50			66,000	42,635.34		
Total body	1,166,654	73,000.00	73,000	0.00	1,352,992	60,000.00	60,000	0.00

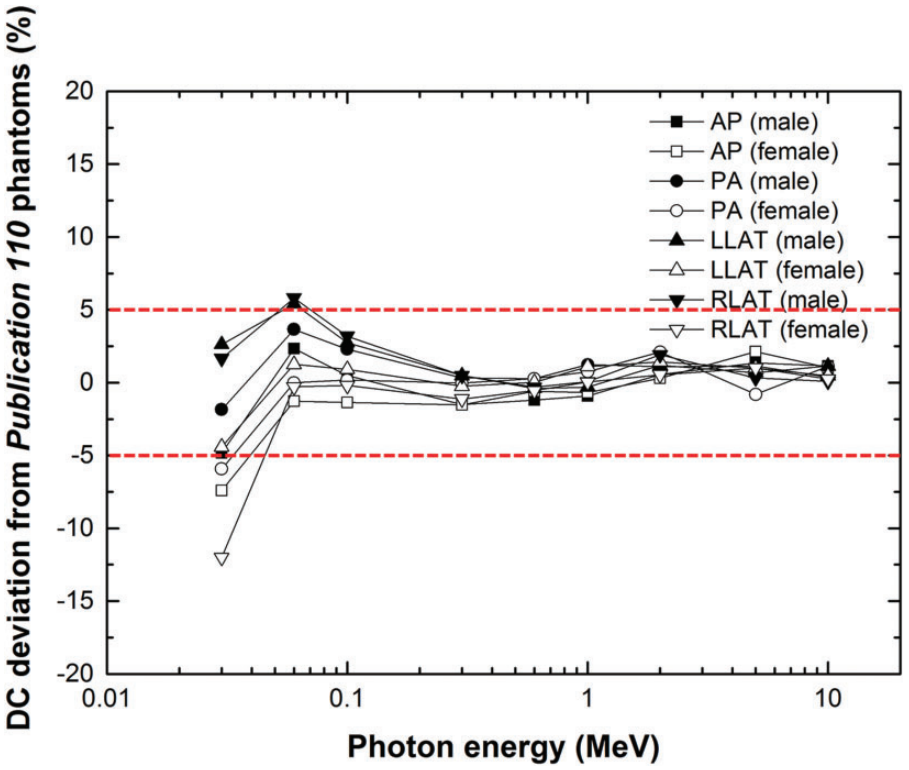

Fig. 2. Deviation of red bone marrow dose coefficients (DCs) of polygon-mesh (PM) version phantoms from those of the *Publication 110* (ICRP, 2009) reference phantoms. DC deviation = {DC (PM) – DC (*Publication 110*)}/DC (*Publication 110*) × 100%. AP, anterior–posterior; PA, posterior–anterior; LLAT, left lateral; RLAT, right lateral.

Fig. 3 shows the dose results for the small intestine for external photon beams. Here, the new PM model, which was developed in the current project, was compared with the previous stylised model. The filled symbols represent the results of the new PM model, and the open symbols represent those of the previous stylised model (Yeom et al., 2013). The overall results show that the new model deviates less from the original voxel model in the *Publication 110* male phantom. The deviations of the new PM model were mostly within 10%.

Fig. 4 shows the electron SAF values of the small intestine calculated by the PM version of the *Publication 110* phantoms developed here and the *Publication 100* (ICRP, 2006) stylised phantoms. The SAF values of the PM phantoms and the stylised phantoms were also calculated using Geant4, but, in this case, the secondary production cut value was reduced to 1 μm considering the micron-thick target regions. The data show that the models of the small intestine of the PM phantoms provide SAF values that are very similar to those of the *Publication 100* stylised

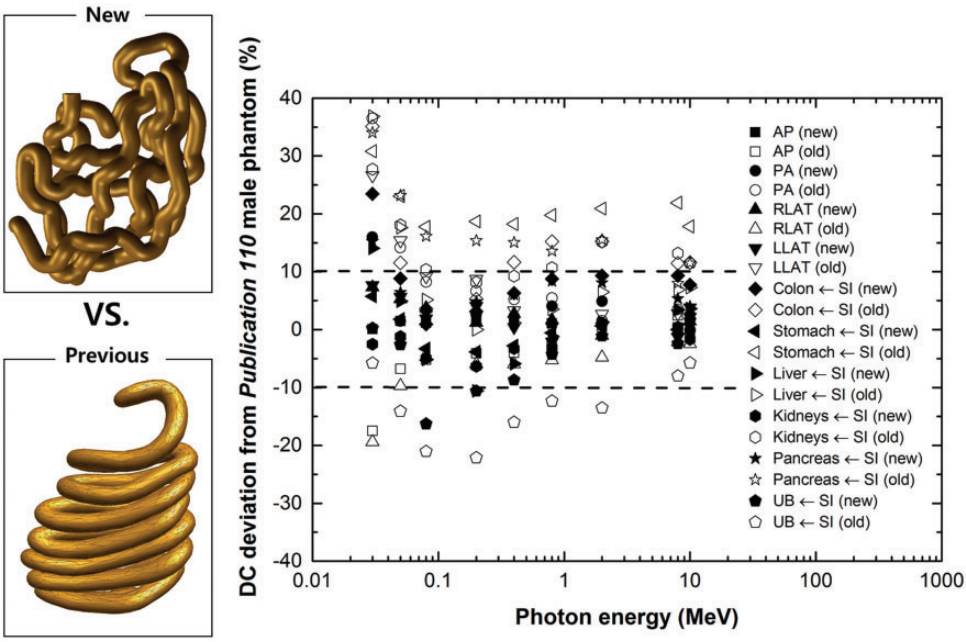

Fig. 3. Deviation of small intestine dose coefficients (DCs) from those of the *Publication 110* (ICRP, 2009) male phantom for the model of the small intestine developed here (filled markers) and for earlier stylised models of the small intestine (unfilled markers) (Yeom et al., 2013). DC deviation = {DC (PM) – DC (*Publication 110*)}/DC (*Publication 110*) × 100%. AP, anterior–posterior; PA, posterior–anterior; LLAT, left lateral; RLAT, right lateral; SI, small intestine; UB, urinary bladder.

phantoms. The results for other alimentary tract organs show very similar trends. These results generally suggest that, in the future, after successful completion of the PM-based reference phantoms, additional stylised phantoms will not be needed for SAF calculations for alimentary tract organs as the PM phantoms will suffice in providing very similar SAF values.

Fig. 5 shows the DCs of the lens of the eye (pGy cm^2) calculated for the PM phantoms for external electron exposures and AP irradiation geometry, along with the corresponding *Publication 116* DCs (ICRP, 2010). The latter were obtained for electrons from 100 keV to 10 MeV using a stylised eye phantom (Behrens et al., 2010), and for all other energies using the *Publication 110* reference phantoms. In order to save computation time, it was assumed that only the head of each phantom is irradiated, and that the contribution of secondary radiations to the dose to the lens of the eye from the other part of the body is negligible. These results demonstrate that the new PM phantoms provide dose values very similar to those of *Publication 116*, even for those energies for which the stylised model was used.

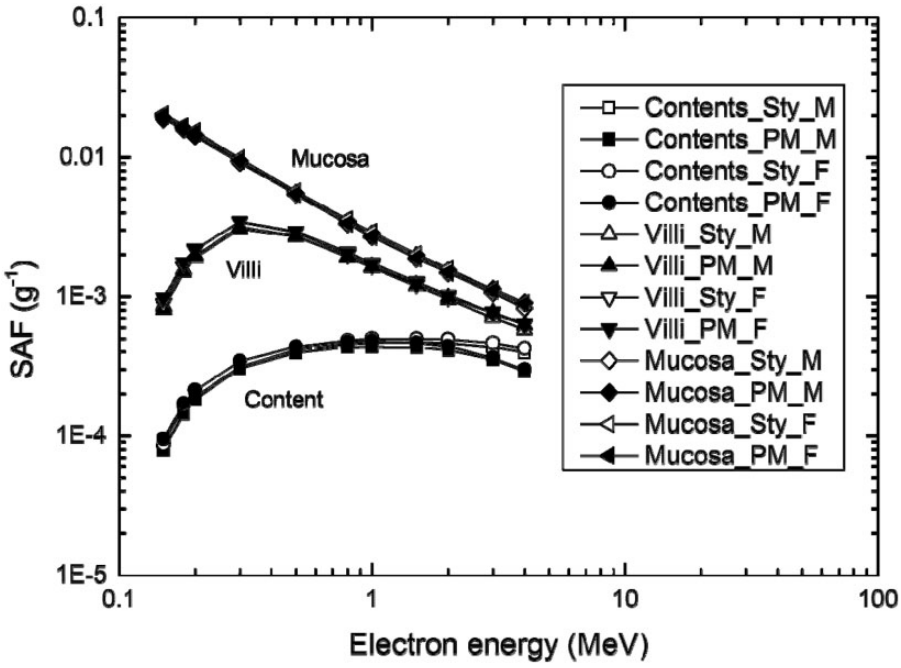

Fig. 4. Specific absorbed fractions (SAFs) for tissues of the small intestine, calculated using the polygon-mesh (PM) phantoms developed in the present study and the *Publication 100* stylised phantoms (ICRP, 2006).

For low-energy electrons (less than 0.7 MeV), the DCs calculated with the current PM phantoms were higher than the *Publication 116* data (maximum difference of 60% at 0.2 MeV). This relatively large difference is caused by the fact that the *Publication 116* data were calculated using the bare-eye model for electron energies of $\leq$10 MeV, and therefore do not properly reflect the dose contribution from the secondary radiations from the head structure. This result confirms that use of an additional stylised phantom for dose calculations for the lens of the eye will not be necessary in the future.

4. CONCLUSIONS

ICRP is currently developing PM versions of the *Publication 110* adult reference phantoms. The final phantoms will include, among the organs and tissues for effective dose calculation, continuous and fully-enclosed layers for the skin and the walls of the stomach, gall bladder, and urinary bladder; thin target layers (8–40 μm) of the respiratory and alimentary tract organs; and detailed and anatomically more accurate models of the skeletal system, lens of the eye, lymphatic nodes, blood vessels, hands, and feet. It is expected that the developed phantoms would provide dose

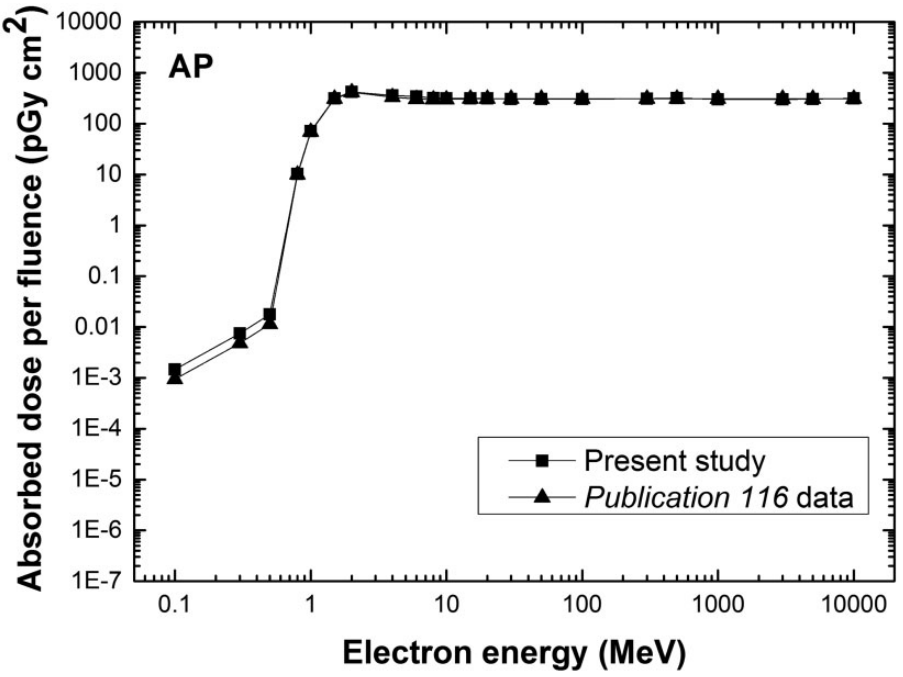

Fig. 5. Absorbed dose for the lens of the eye per fluence (pGy cm^2) for electron exposures in anterior–posterior (AP) irradiation geometry, as calculated for the present study with the polygon-mesh phantoms (square) and *Publication 116* data (triangle) (ICRP, 2010). The calculated dose values are for the entire lens and present mean values of both eyes and both sexes.

values very similar to those of the current *Publication 110* reference phantoms for highly penetrating radiations, and more accurate or correct dose values for weakly penetrating radiations (electrons, ions, and low-energy photons <0.03 MeV) and small tissues. Additionally, the developed phantoms would be deformable, providing different postures (e.g. walking and sitting) for calculation of DCs in emergency exposure scenarios, which is planned for the next term of Committee 2 (2017–2021). The project is expected to provide all-in-one, deformable, high-quality PM phantoms representing the reference male and female adults for the radiological protection community.

REFERENCES

Agostinelli, S., Allison, J., Amako, K., et al., 2003. GEANT4 – a simulation toolkit. Nucl. Instrum. Meth. A506, 250–303.

Behrens, R., Dietze, G., Zankl, M., 2009. Dose conversion coefficients for electron exposure of the human eye lens. Phys. Med. Biol. 54, 4069–4087.

Behrens, R., Dietze, G., Zankl, M., 2010. Corrigendum – Dose conversion coefficients for electron exposure of the human eye lens. Phys. Med. Biol. 55, 3937–3945.

Cullen, D., Hubbell, J.H., Kissel, L., 1997. EPDL97: the Evaluated Photon Data Library, 1997 Version. UCRL-50400, Vol. 6, Rev. 5. Lawrence Livermore National Laboratory, Livermore, CA.

Dice, L., 1945. Measures of the amount of ecologic association between species. Ecology 26, 297–302.

Edelsbrunner, H., Kirkpatrick, D.G., Seidel, R., 1983. On the shape of a set of points in the plane. IEEE Trans. Inf. Theory 29, 551–559.

ICRP, 1994. Human respiratory tract model for radiological protection. ICRP Publication 66. Ann. ICRP 24(1–3).

ICRP, 2002. Basic anatomical and physiological data for use in radiological protection reference values. ICRP Publication 89. Ann. ICRP 32(3/4).

ICRP, 2006. Human alimentary tract model for radiological protection. ICRP Publication 100. Ann. ICRP 36(1/2).

ICRP, 2007. The 2007 Recommendations of the International Commission on Radiological Protection. ICRP Publication 103. Ann. ICRP 37(2–4).

ICRP, 2009. Adult reference computational phantoms. ICRP Publication 110. Ann. ICRP 39(2).

ICRP, 2010. Conversion coefficients for radiological protection quantities for external radiation exposures. ICRP Publication 116. Ann. ICRP 40(2–5).

Lee, C., Kaufman, K., Pafundi, D.H., et al., 2009. An algorithm for lymphatic node placement in hybrid computational phantoms – applications to radionuclide therapy dosimetry. Proc. IEEE 97, 2098–2108.

Lee, C., Lodwick, D., Hurtado, J., et al., 2010. The UF family of reference hybrid phantoms for computational radiation dosimetry. Phys. Med. Biol. 55, 339–363.

Nguyen, T.T., Yeom, Y.S., Kim, H.S., et al., 2015. Incorporation of detailed eye model into polygon-mesh versions of ICRP-110 reference phantoms. Phys. Med. Biol. 60, 8695–8707.

Perkins, S.T., Cullen, D.E., Seltzer, S.M., 1991. Tables and Graphs of Electron-Interaction Cross-Sections from 10 eV to 100 GeV Derived from the LLNL Evaluated Electron Data Library (EEDL), Z = 1–100. UCRL-50400, Vol. 31. Lawrence Livermore National Laboratory, Livermore, CA.

Perkins, S.T., Cullen, D.E., Chen, M.H., Hubbell, J.H., Rathkopf, J., Scofield, J., 1997. Tables and Graphs of Atomic Subshell and Relaxation Data Derived from the LLNL Evaluated Atomic Data Library (EADL), Z = 1–100. UCRL-50400, Vol. 30. Lawrence Livermore National Laboratory, Livermore, CA.

Shin, D.S., Chung, M.S., Park, J.S., et al., 2012. Portable document format file showing the surface models of cadaver whole body. J. Korean Med. Sci. 27, 849–856.

Yeom, Y.S., Han, M.C., Kim, C.H., et al., 2013. Conversion of ICRP male reference phantom to polygon-surface phantom. Phys. Med. Biol. 58, 6985–7007.

Yeom, Y.S., Kim, H.S., Nguyen, T.T., et al., 2015. New small-intestine modeling method for surface-based computational human phantoms. J. Radiol. Prot. (submitted).